DOI: 10.13009/EUCASS2019-869

Supersonic vortex wake at a wide distance from the wing and influence of acoustic type waves

V.E. Borisov[1], A.A. Davydov[2]*, T.V. Konstantinovskaya[3]*, A.E. Lutsky[4]*, A.M. Shevchenko[5]**, A.S. Shmakov[6]***

**Keldysh Institute of Applied Mathematics RAS*

Miusskaya sq., 4, Moscow, Russia, 125047

[1]narelen@gmail.com, [2]ryzhiy@list.ru, [3]konstantinovskaya.t.v@gmail.com, [4]allutsky@yandex.ru

***Khristianovich Institute of Theoretical and Applied Mechanics SB RAS*

Institutskaya str., 4/1, Novosibirsk, Russia, 630090

[5]shevch@itam.nsc.ru, [6]shmakov@itam.nsc.ru

Abstract

The supersonic flow behind a wingtip vortex generator in a steady state inlet flow and in a flow influenced by acoustic type waves was studied numerically and experimentally. The wing attack angle was 10 degrees, the incoming flow Mach number was M_∞ = 2, 3 and 4. The numerical data were obtained in the wide region exceeding 30 chords downstream from the wing. Quantitative experimental data were obtained in two cross sections at a distance of 2 and 6 chords downstream from the wing for steady state inlet flow. A comparative analysis of the results was carried out.

1. Introduction

The flight of any aircraft in the atmosphere is accompanied by the formation of a vortex wake. The study of this problem is important from the point of view of the aircraft traffic organization, including passenger air transportation, since the encounter of one aircraft in the vortex wake left by another aircraft can be extremely dangerous. In such situation an intensive roll motion may develops, which can lead to an involuntary change of course, altitude, etc. up to total loss of control. One of these accidents occurred in January 2017 when a private jet (Bombardier Challenger 604) flipped several times and plummeted more than 3000 metres and rolled uncontrollably after its encountering with wake turbulence from an Airbus A380 flying above it before the pilot could regain control [1]. For supersonic aircraft, an additional danger and interest for study is the possible entry of a wingtip vortex into other parts of the aircraft.

Due to the introduction of conceptually new aircrafts, despite existence of earlier works, more in-depth study of vortex wake is necessary for further development of civil and military aviation, including a research at the supersonic modes.

Numerical methods for calculations of turbulent flow, in particular for calculations of wingtip vortices, actively develop in view of the increasing efficiency of computing systems, giving the possibility to pursue more detailed and extensive numerical researches.

Thus, investigation of formation and evolution of wingtip vortices is an important problem of aerogasdynamics. Solution of this problem makes it possible to use it for solving a number of practical challenges [2, 3]. Extensive reviews of papers devoted to the studies of the structure and behaviour of wingtip vortices were given in [4], [5] and [6]. Some experimental data for supersonic modes can be found in [7-11], and numerical data – in [12]. Therefore, the first aim of this work is to investigate a supersonic wingtip vortex in a steady state incoming flow in a wide flow region.

Another problem that has a great theoretical and practical interest [13], especially with regard to the exploitation of high-speed aircrafts, is the understanding of the incoming flow disturbance influence on the flow parameters at supersonic flow around solid bodies. This interest is caused, firstly, by widespread presence of acoustic waves or acoustic noise at the atmosphere, and secondly, by existence of an acoustic background in a test section of wind tunnels during the tests [14, 15].

Many authors have studied the influence of disturbances on the boundary layer. In particular, an extensive work has been carried out to study the influence of disturbances on the change of the boundary layer parameters on a flat plate and on a wedge in a supersonic flow [16, 17]. Another work devoted to study of boundary layer receptivity on a flared cone to freestream disturbance in hypersonic flow [18].

DOI: 10.13009/EUCASS2019-869

The investigation of the perturbations influence on the wingtip vortex is no less interesting, but this question is still insufficiently studied. Earlier the authors of present paper have investigated a vortex wake behind a wing in a supersonic flow in the absence of disturbances [19]. Hence, the second aim of this work is to determine the effect of acoustic type disturbances on the wingtip vortex parameters in a supersonic flow.
In this work the supersonic flow behind a wing – wingtip vortex generator was studied. The wing was straight with sharp leading and trailing edges. In all simulations the wing attack angle was 10 degrees.
In the first part of the work the case of a steady state inlet flow was numerically and experimentally investigated. The Mach number of the incoming flow was M_∞ = 2, 3 and 4.
In the second part of the work a flow influenced by acoustic type waves was numerically investigated. The Mach number of the incoming flow was M_∞ = 2 and 3. Acoustic type disturbances were introduced in steady state incoming flow in the form of a monochromatic plane wave with small amplitude in which all values are simple periodic functions of time. This allows us not to limit the generality, since any sound wave can be represented as a superposition of monochromatic plane waves with different wave vectors and frequencies [20]. For this aim a Fourier analysis can be used that allows to get a spectral representation of a wave perturbation.
The CFD simulations have been performed at the Keldysh Institute of Applied Mathematics RAS using up to 896 cores on the hybrid multiprocessor computer system K-60 [21]. An approach based on the URANS method with the SA turbulence model was applied. The numerical data were obtained in the wide region exceeding 30 chords downstream from the wing.
The experiments have been performed in a supersonic wind tunnel T-325 at Khristianovich Institute of Theoretical and Applied Mechanics SB RAS. The shadow visualization of the flow and the measurement of the mass flow distribution with the help of a thermoanemometer have been carried out. Quantitative experimental data were obtained in two cross sections that are perpendicular to the velocity vector of the incoming flow at a distance of 2 and 6 chords downstream from the longitudinal axis of the wing.
Detailed numerical and experimental data has been obtained on the position and dimensions of the vortex core and of its axis with quantitative data on the distribution of flow gas-dynamic characteristics. A comparative analysis of numerical results and experimental data was performed.
A numerical data on the gasdynamic parameters pulsation in the vortex wake influenced by the acoustic type disturbance are obtained, in particular, frequencies and disturbance ranges on the wingtip vortex axis are investigated depending on a distance from the wing - vortex generator.
This study is a continuation of previous works of the authors [22, 23, 19].

2. Model description

2.1 Geometry

The wing – wingtip vortex generator was straight with sharp leading and trailing edges. The wing had a diamond-shaped base, a chord *b* = 30 mm, a half-span 95 mm (fig. 1-a). The wing attack angle was 10 degrees.
In numerical simulations the incoming flow Mach number was M_∞ = 2, 3 and 4 and Reynolds number was

$Re = 1 \cdot 10^7$ [m^{-1}].

(a) (b) (c)

Figure 1: Wing – generator model scheme: experimental facility (a), model (b) numerical interpretation with surface mesh (c)

DOI: 10.13009/EUCASS2019-869

The experiments have been performed in a supersonic wind tunnel T-325 at Khristianovich Institute of Theoretical and Applied Mechanics SB RAS. The shadow visualization of the flow and the measurement of the mass flow distribution have been carried out with the help of a thermoanemometer. For Mach number $M_\infty = 2$, the experiments were carried out at unit Reynolds numbers of 4 and 11 million per meter, for $M_\infty = 3$, the unit Reynolds number was 9, 15 and 18 million per meter, for $M_\infty = 4$ - 17.5 million per meter.

2.2 Numerical method

For describing a supersonic flow of a perfect viscous compressible fluid we used a system of unsteady Reynolds averaged Navier–Stokes equations (URANS) with the one-parameter Spalart–Allmaras turbulence model for compressible flows [24] with Edwards modification [25]. The finite volume method based on the reconstruction schemes of the second order (TVD) or the third order (WENO) was used. Time approximation was performed by means of an implicit scheme based on the LU-SGS method and by an explicit scheme. A more complete description of the numerical algorithms and the mathematical model used in this paper is given in [26].
The numerical simulations have been performed at the Keldysh Institute of Applied Mathematics RAS using the hybrid supercomputer system K-60 [21]. The numerical data were obtained in the wide region exceeding 30 chords downstream from the longitudinal wing axis.

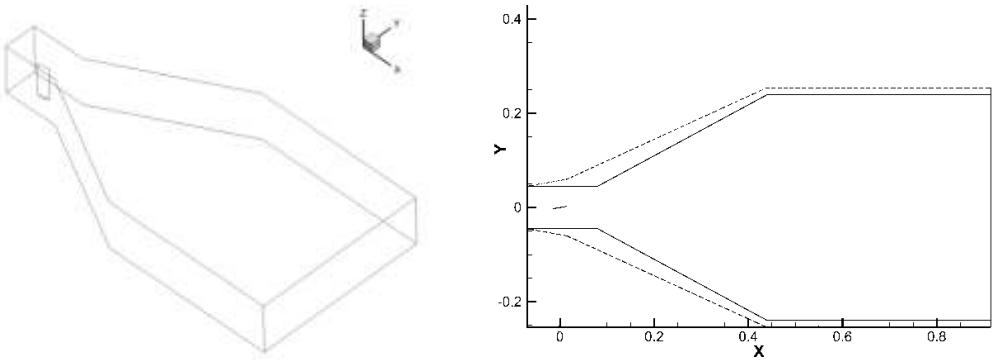

Figure 2: Computational domain (left), extension of external domain boundaries on Y axis (right) for the case of $M_\infty = 2$ (dashed line) with respect to the case of $M_\infty = 3$ and 4 (solid line)

The external boundaries of the calculation area were arranged in such a way as to minimize their influence on the flow parameters. In particular, for numerical simulations with the incoming flow Mach number $M_\infty = 2$, the boundaries of the computational domain were extended along the coordinate Y with respect to the numerical simulations for $M_\infty = 3$ and $M_\infty = 4$ (fig. 2).
An unstructured grid with hexagonal cells was used. Number of cells was 15 572 304 for Mach number $M_\infty = 2$ and 15 296 688 for Mach number $M_\infty = 3$ and 4. The grid was thickened in the zone of vortex formation (especially near the tip chord of the wing, fig. 1 – b) and in the zone of the wingtip vortex throughout all simulation area, that allowed for more accurate simulations.

2.3 Efficiency of parallel algorithm

During our work an investigation of employed parallel implicit algorithm efficiency depending on the number of used cores was performed also. Its results are presented in Table 1. For this investigation speedup S_p and efficiency E_p were found, which are expressed by: $S_p = T_1/T_p$, $E_p = S_p/p$, where T_1 is executing time of the parallel algorithm on one core, T_p is executing time of the parallel algorithm on p cores.
The calculation of speedup and efficiency was performed on 1, 28, 56, 112, 224, 448 and 896 cores. The same grid has been used. Thousand steps were performed from one computational point at Mach number $M_\infty = 4$. Used parallel algorithm shows a high efficiency which does not become less than 0.478 even when using up to 896 cores (table 1). The main results were obtained on 112 cores.

DOI: 10.13009/EUCASS2019-869

Table 1: Efficiency and speedup of the used parallel algorithm

p	execution time (sec)	S_p	$E_p(\%)$
1	41490.660		
28	2045.038	20.3	72.5
56	1006.938	41.2	73.5
112	571.426	72.6	64.8
224	283.676	146.3	65.3
448	179.135	231.6	51.7
896	96.829	428.5	47.8

With the increase in the number of used cores, the efficiency of parallel implementation of the numerical algorithm decreases (see table 1), that is obviously, since with the increase in the number of cores the number of exchanges increases, and the amount of arithmetic computation on each core decreases. This leads to an unfavorable relationship between the volume of data transferred between the cores and the amount of produced computations.

3. The results for steady state incoming flow

At the condition of steady state incoming flow detailed numerical-experimental data has been obtained on the position and dimensions of the vortex core with quantitative data on the distribution of gas-dynamic characteristics of the flow.

A comparative analysis of the results of numerical and experimental simulation has shown that for all the cases considered the wingtip vortex is characterized by a minimum of such quantities as density, pressure (fig. 3 – a), longitudinal Mach number M_x, by increase in the static temperature and by a maximum of helicity H (fig. 3 – b) on its axis. The maximum of the tangential Mach number M_{yz} (fig. 3 – c) and of mass flow are fixed at the boundary of the wingtip vortex. Gas-dynamic values along a line passing through the vortex axis are presented in figure 3.

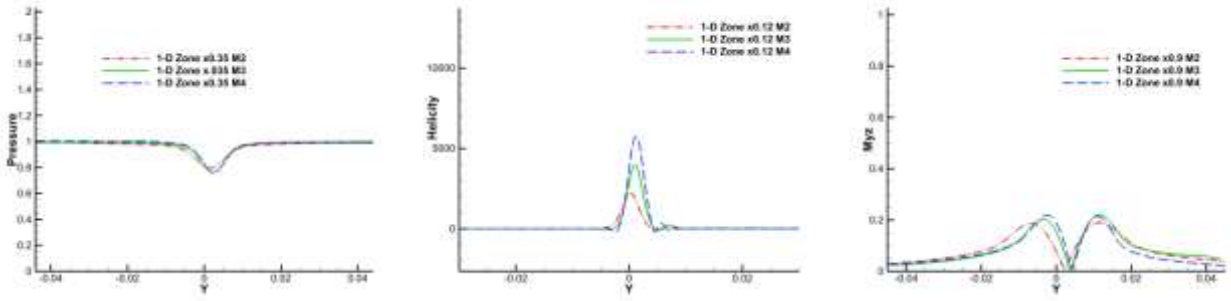

(a) (b) (c)

Figure 3: Gas-dynamic values at the vortex wake across the vortex axis for some cross sections of the fixed coordinate x for all considered M_∞: pressure at x = 0.12 (a), helicity at x = 0.35 (b), tangential Mach number M_{yz} at x = 0.9 (c)

3.1 Numerical results

The wingtip vortex begins with its formation on the lateral edge of the wing. High pressure air from the lower surface of the wings flows around the wingtip to the lower pressure air region above the wings forming wingtip vortices. This process is clearly distinguishable from the obtained numerical results (fig. 4).

After its formation the wingtip vortex develops in the form of such a longitudinal structure (fig. 5) possessing certain properties.

DOI: 10.13009/EUCASS2019-869

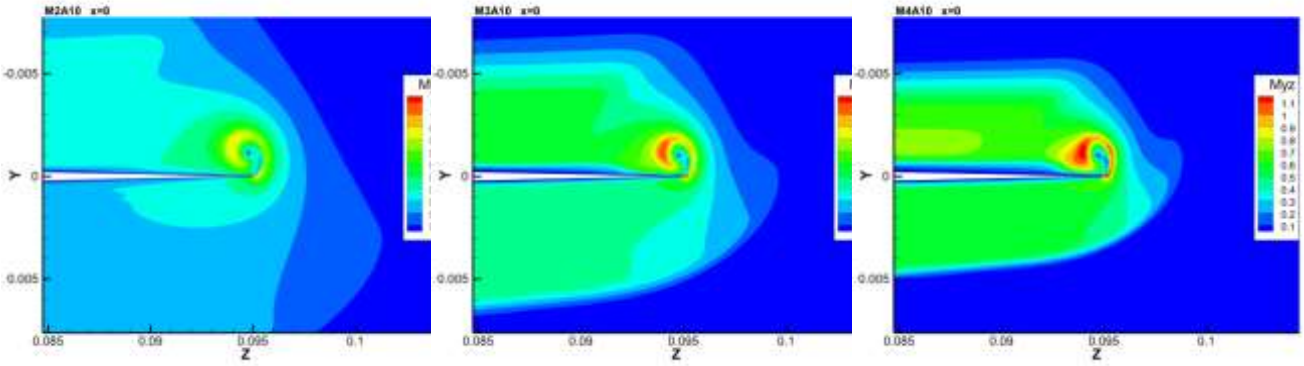

(a) (b) (c)

Figure 4: Vortex formation on a tip chord described in terms of the tangential Mach number M_{yz} in the cross section passing through longitudinal wing axis: $M_\infty = 2$ (a), $M_\infty = 3$ (b) and $M_\infty = 4$ (c)

The significant characteristics of a wingtip vortex are its properties on its axis. The figure 6 illustrates method of wingtip vortex axis coordinates detection in experimental data by a minimum of the relative mass flow applied in section of $x/b = 2$. In numerical data the position of wingtip vortex axis was obtained similarly by a minimum of the tangential Mach number M_{yz}.

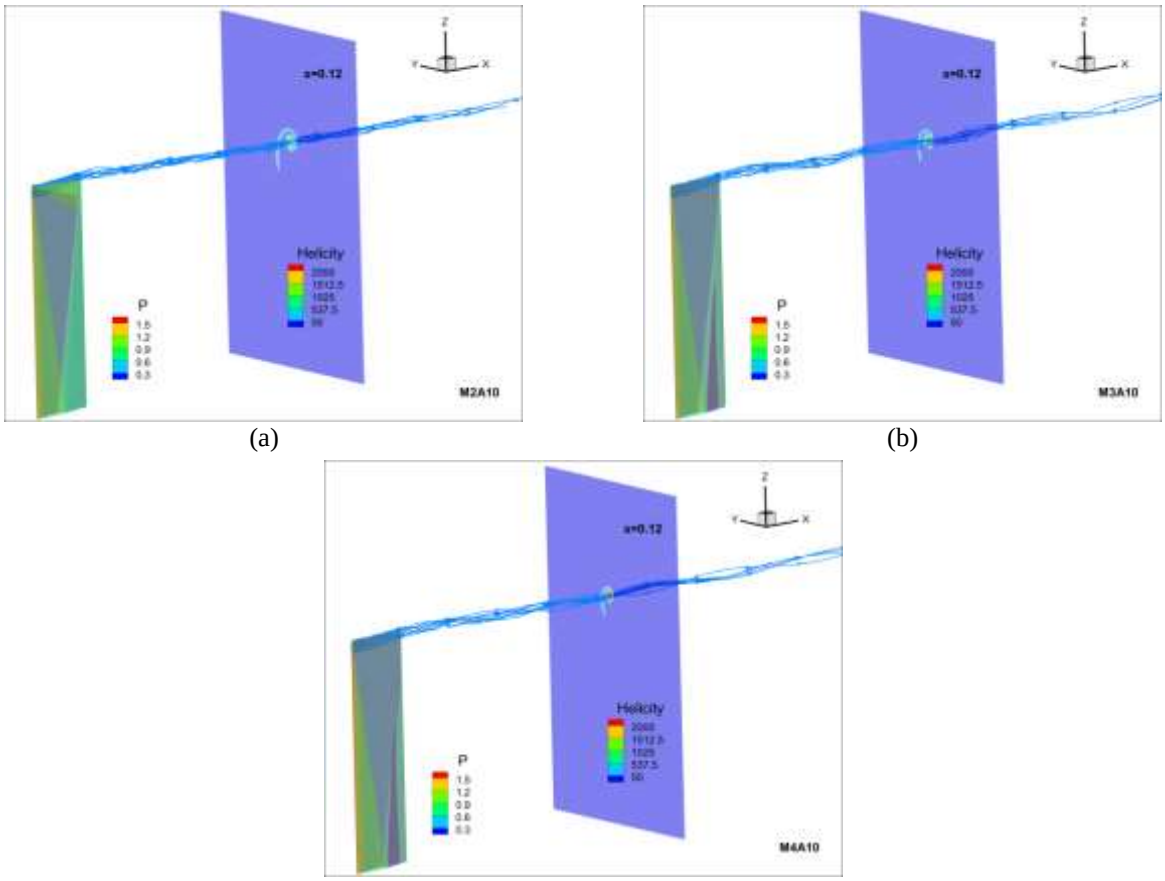

(a) (b)

(c)

Figure 5: The wing-generator with a pressure on it, streamtraces passing through/near the wingtip and helicity in the cross section $x = 0.12$ for: $M_\infty = 2$ (a), $M_\infty = 3$ (b) and $M_\infty = 4$ (c)

DOI: 10.13009/EUCASS2019-869

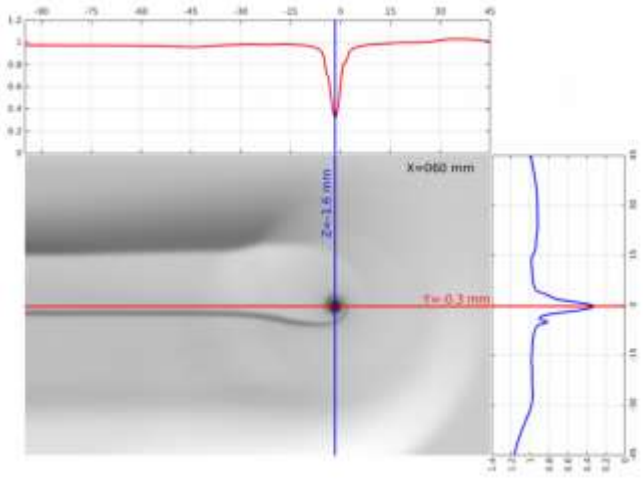

Figure 6: Detection of vortex axis position in experimental data by means of relative mass flow minimum

Wingtip vortex intensity is a principal characteristic of the vortex that is reflected in values of gas-dynamic parameters in the vortex region and on its axis.

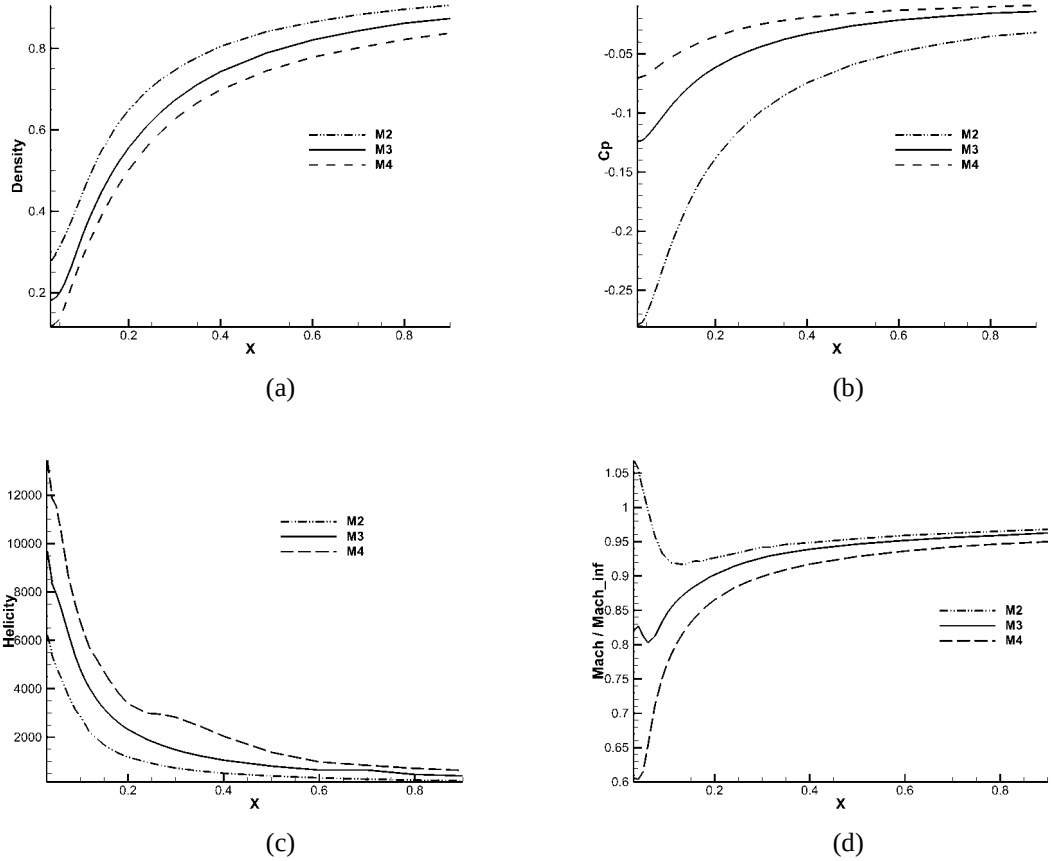

Figure 7: Gas-dynamics parameters on wingtip vortex axis along the coordinate *x*: density ρ (a) pressure coefficient *Cp* (b), helicity *H* (c) and normalized Mach number (d)

Pressure coefficient C_p and helicity H are expressed by following formulae: $C_p = (P-P_\infty)/(\frac{1}{2}\rho_\infty \mathbf{V}^2_\infty)$, $H = \mathbf{V} \cdot \nabla \times \mathbf{V}$ where $\mathbf{V}$ is a velocity vector, P is a pressure, ρ is a density. Helicity have a topological interpretation as a measure of vortex lines knottedness in the flow.

DOI: 10.13009/EUCASS2019-869

With increasing coordinate *x* (i.e., downstream from the wing), the intensity of the wingtip vortex decreases for all the incoming flow Mach numbers considered, which is accompanied, for example, by an increasing in pressure coefficient and by a decreasing in helicity (fig. 7 – b – c), which tend to reach the values of undisturbed flow at the end of the computational region. It is also obtained that in the case of Mach number $M_\infty = 2$ there is a zone behind a wing where velocity on wingtip vortex axis is higher, than a main flow velocity (fig. 7 – d), thus there is jet-like flow.

Among other parameters a pressure distribution normalized by free stream pressure is obtained in the calculation domain. The pressure field at the transversal sections of fixed coordinate *x* is shown in the figure 8. This figure also shows a zone of wingtip vortex formation (fig. 8 – a – e – i), a wingtip vortex evolution and intensity, the vortex core.

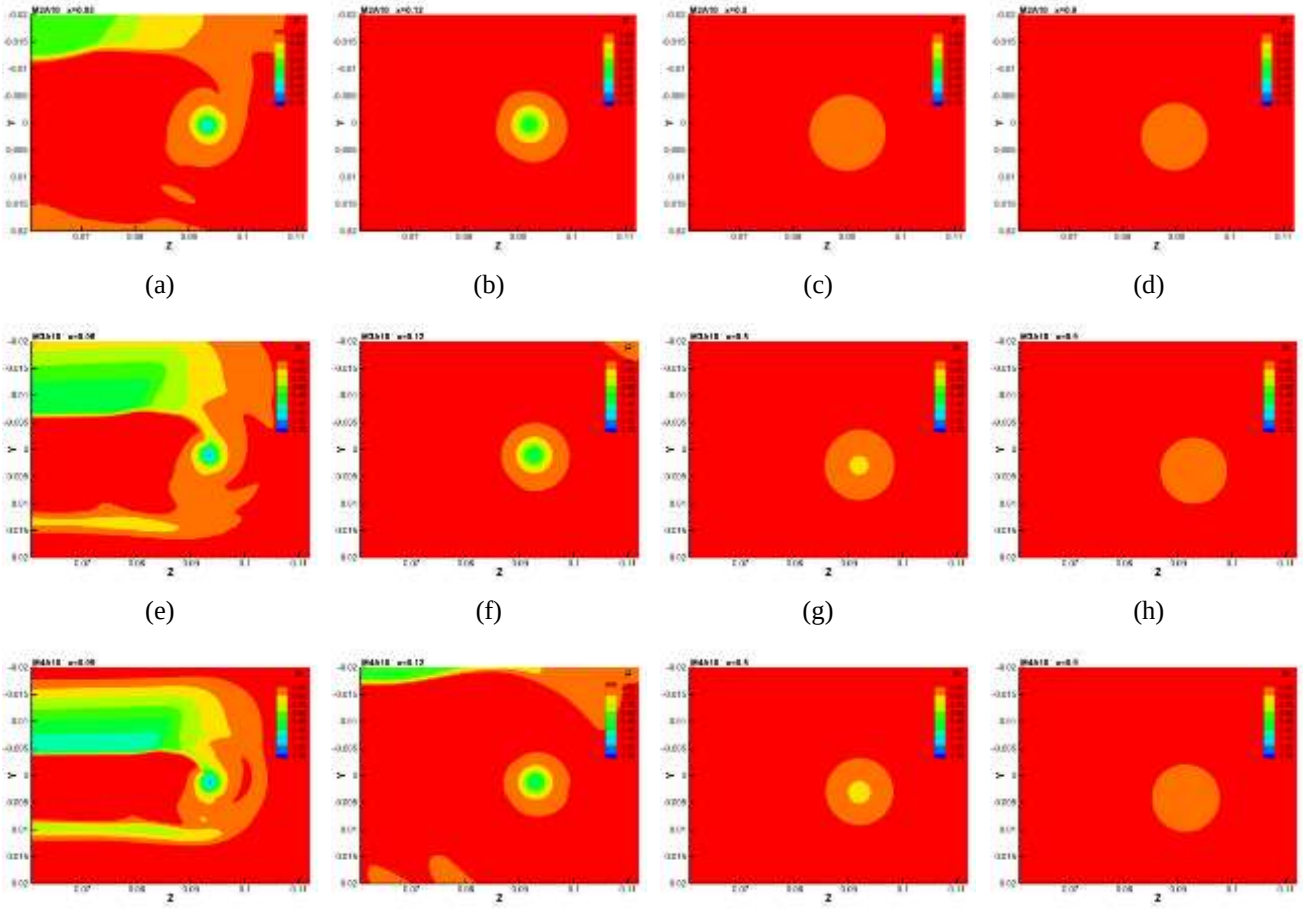

(a) (b) (c) (d)

(e) (f) (g) (h)

(i) (j) (k) (l)

Figure 8: Pressure distribution in cross-sections of fixed coordinate *x*: $M_\infty = 2$: $x = 0.05$ (a), $x = 0.12$ (b), $x = 0.5$ (c), $x = 0.9$ (d); $M_\infty = 3$: $x = 0.05$ (e), $x = 0.12$ (f), $x = 0.5$ (g), $x = 0.9$ (h); $M_\infty = 4$: $x = 0.05$ (i), $x = 0.12$ (j), $x = 0.5$ (k), $x = 0.9$ (l)

In calculation domain the more is the incoming flow Mach number the more intensive is the wingtip vortex (fig. 8). Intensity of vortices decrease with the distance from the wing – generator for all incoming flow Mach numbers considered.

3.2 Comparison of numerical and experimental data

The geometry of the tests was the same as in the numerical simulations (fig. 1). The scheme of the experiment is shown in fig. 1. The experimental procedure is presented in more detail in [10, 11].

A distribution of mass flow at the wingtip vortex and at its vicinity along the horizontal coordinate *z* in the cross section $x/b = 2$ for Mach number $M_\infty = 2$ and $M_\infty = 3$ is presented in the figure 9. This plots show a satisfactory agreement between the numerical simulations result and the experimental data. It should be noted that in the

DOI: 10.13009/EUCASS2019-869

experimental data the dependence of results on a Reynolds number is observed. This question is the subject of further research.

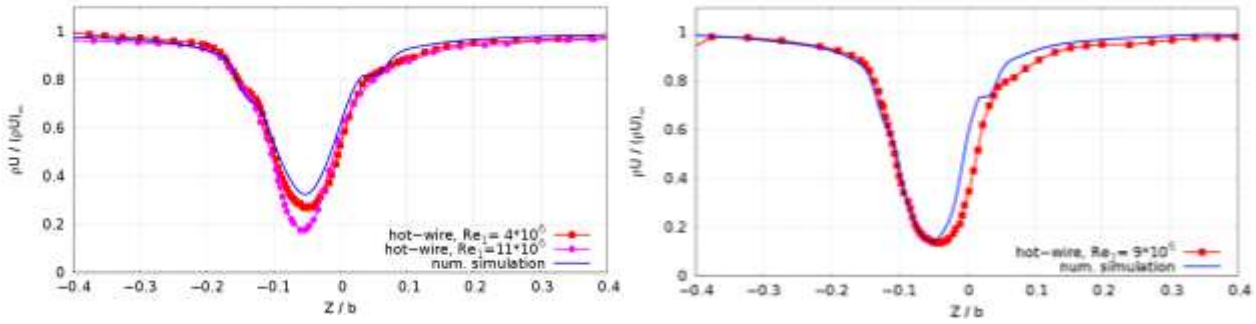

(a) (b)

Figure 9: Distribution of mass flow at the wingtip vortex and at its vicinity along the horizontal coordinate *z* in the cross section *x/b* = 2 at M_∞ = 2 (a) and M_∞ = 3 (b)

Figure 10 shows a comparison of the distribution of root-mean-square pulsations of mass flow (m ') (experimental data) with the tangential Mach number (M_{yz}) (numerical data) in the core of the wingtip vortex and its vicinity for M_∞ = 3 and at *x /b* = 2. As well known, the mass flow pulsations and the circumferential velocity (and the corresponding tangential Mach number M_{yz}) are maximal at the boundary of the vortex core. In the center, on the contrary, these values are minimal (in the ideal case, M_{yz} = 0) [7, 27, 28]. As can be seen, the coordinates of the maxima and minima of the quantities M_{yz} (simulation) and m '(experiment) coincide. This indicates a good agreement between the results of the numerical simulation and of the experiment.

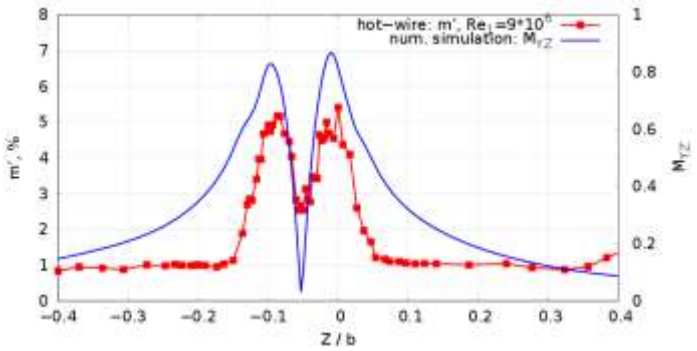

Figure 10: Comparison of mass flow root-mean-square pulsations distribution (m`) and of tangential Mach number (M_{yz}) at the wingtip vortex and at its vicinity along the horizontal coordinate *z* in the cross section *x/b* = 2 at M_∞ = 3

4. Acoustic type disturbance

4.1 Introduced disturbance

Disturbances in the form of a monochromatic plane wave with small amplitude at the inlet boundary were introduced in steady state incoming flow to investigate the effect of acoustic waves:

$$\begin{pmatrix} u' \\ v' \\ p' \\ \rho' \end{pmatrix} = A \begin{pmatrix} \pm\cos\theta \\ \mp\sin\theta \\ 1 \\ 1 \end{pmatrix} \cos\left(k_x x + k_y y - \omega t\right)$$

DOI: 10.13009/EUCASS2019-869

When u', v', p' and ρ' – pulsations of *u* and *v* velocity components, of pressure and of density respectively; θ – angle of wave incidence; A – disturbance amplitude; t – time; $k_x = k\cos\theta$, $k_y = -k\sin\theta$, $k = \omega / (M_\infty \cos\theta \pm 1)$; ω is dimensionless frequency; the upper (lower) sign corresponds to a fast (slow) acoustic wave.

4.2 Numerical results under acoustic wave influence

The disturbance was introduced in steady state incoming flow on the inlet boundary in the form of slow acoustic waves. There were numerically investigated two cases: Mach number $M_\infty = 2$ and dimensionless frequency $\omega = 100$, Mach number $M_\infty = 3$ and $\omega = 100$. Amplitude of the introduced disturbances was $A = 0.0286 \cdot P_\infty$ and angle of wave incidence was $\theta = 0$.

The general view of the pressure field in the longitudinal section $z = 0.093$ (for tip chord $z = 0.095$) along the calculation domain is shown on the figure 11, the results for the $M_\infty = 2$ are presented: (a) under steady state incoming flow; in the presence of slow acoustic type waves at $\omega = 100$ (b). In the middle of each part of the figure 11, a zone of the wingtip vortex wake formed behind the wing-generator is distinguished due to low pressure values on it: the vortex zone in steady state incoming flow (fig. 11 – a) and under the influence of disturbance with $\omega = 100$ (fig. 11 – b). Pressure legends are different because otherwise the disturbances are not visible against the background of the free flow pressure.

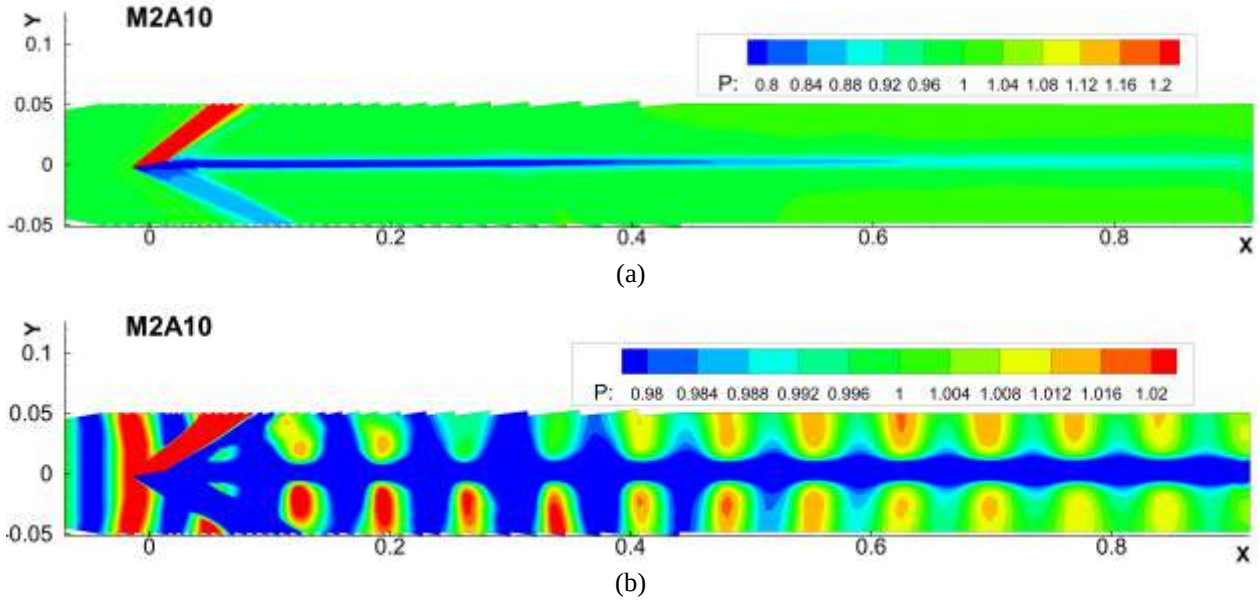

Figure 11: The pressure field in the longitudinal section $z = 0.093$ for $M_\infty = 2$ and $\omega = 100$: (a) steady state incoming flow; (b) incoming flow with slow acoustic type disturbances

Fluctuations of pressure in several points on the vortex axis are presented in the figure 12. The coordinate *x* of the points is equal to 0.2, 0.5 and 0.9 (figure 12 – a, 12 – b and 12 – c respectively). The solid line represents pressure for Mach number $M_\infty = 3$, dash-dot-dotted line represents pressure for Mach number $M_\infty = 2$. It is seen that the amplitude of the pressure fluctuation decreases with distance downstream from the wing (i.e. from the inlet boundary). This is natural, because the presence of viscosity leads to the dissipation of the sound waves energy, therefore the sound is absorbed, i.e. its intensity gradually decreases [20]. It can also be noted that the amplitude of the pressure fluctuations at the Mach number $M_\infty = 3$ is greater than at the Mach number $M_\infty = 2$ which is explained by the greater flow rate.

DOI: 10.13009/EUCASS2019-869

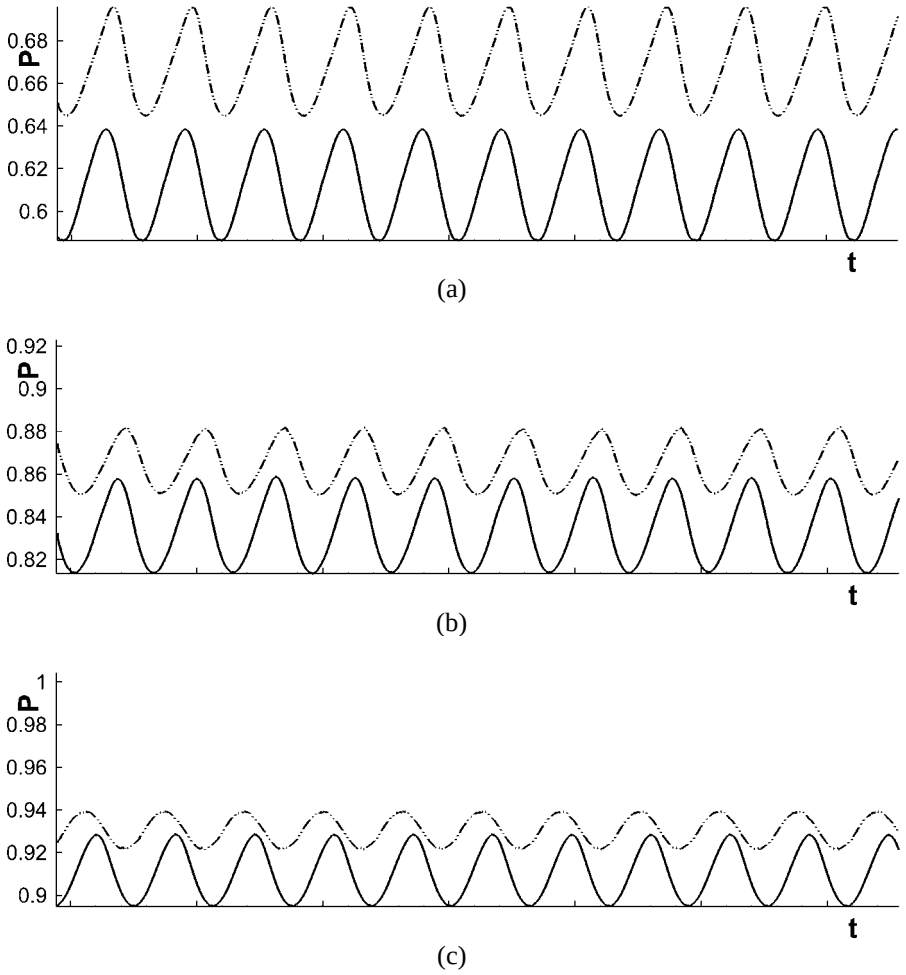

Figure 12: Pressure fluctuations in few points on the vortex axis at the different coordinate x for $M_\infty = 2$ (dash-do-dotted line) and $M_\infty = 3$ (solid line): (a) $x = 0.2$; (b) $x = 0.5$; (c) $x = 0.9$

4.3 Spectral analysis

The discrete Fourier transform (DFT) was used for spectral analysis to processing the obtained numerical results [29, 30]. A set of values obtained as a result of periodic sampling of a continuous signal in the time domain was used as a discrete signal [31].

On the figures 13, 14 and 15 the results of spectral analysis of numerical data are presented, namely the amplitude spectrum of the pressure in the several points on the wingtip vortex axis. The coordinate x of those points equals to 0.2, 0.5 and 0.9 (figure 13, 14 and 15 respectively). The results are presented for two cases considered: incoming flow Mach numbers $M_\infty = 2$ (red line) and $M_\infty = 3$ (black line), dimensionless frequency of introduced perturbation is $\omega = 100$.

Figures 13, 14 and 15 show that the first harmonic frequency is preserved when perturbations move across computational region and coincides with the frequency of the introduced perturbation at the boundary of the region. There are additional harmonics with frequencies that are multiple of the first harmonic frequency in the first half of the region after wingtip vortex formation (figures 13 and 14). Their amplitudes are small. Overall, the amplitudes of the corresponding pressure fluctuation frequencies are greater for the Mach number $M_\infty = 3$ than for the $M_\infty = 2$. However, the amplitude of the second harmonic on the vortex axis is greater for the Mach number $M_\infty = 2$ than for the $M_\infty = 3$ at $x = 0.2$ (fig. 13). Amplitudes of all harmonics decrease when moving towards the end of the computational domain. Additional harmonics disappear by the end of the computational domain for the case of Mach number $M_\infty = 2$, but for the case of Mach number $M_\infty = 3$ the second harmonic has a small contribution even at the end of the region (fig. 15). Therefore first harmonic play primary role in the influence process.

As mentioned above, pressure fluctuations amplitude decreases due to sound adsorption. This is demonstrated on the figure 16 where the amplitude spectrum of the pressure fluctuation on the vortex axis at $x = 0.5$ for the case of

DOI: 10.13009/EUCASS2019-869

incoming flow Mach number 2 and dimensionless frequency ω = 300 is presented calculated both by URANS and by Euler equations.

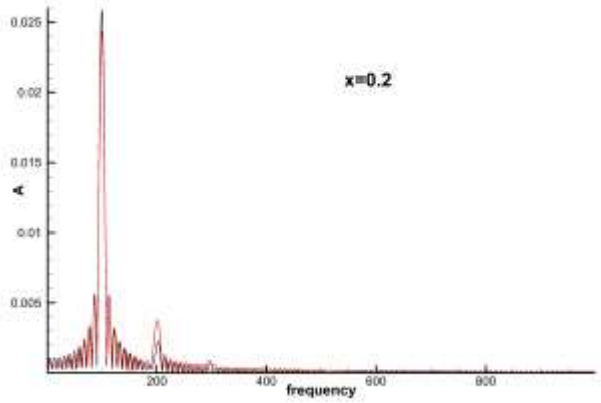

Figure 13: Amplitude spectrum of pressure *P* in a point on the vortex axis at the coordinate *x* = 0.2: incoming flow Mach number M_∞ = 2 (red line) and M_∞ = 3 (black line)

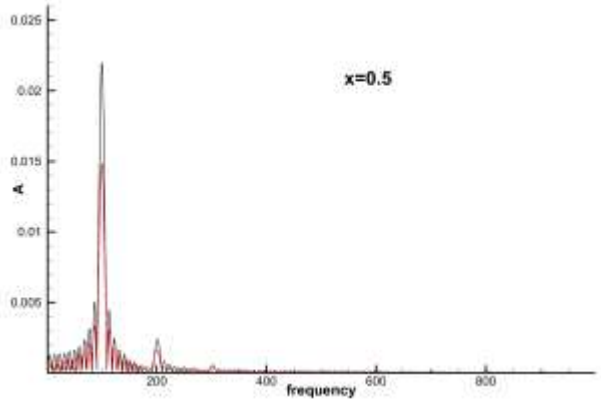

Figure 14: Amplitude spectrum of pressure *P* in a point on the vortex axis at the coordinate *x* = 0.5: incoming flow Mach number M_∞ = 2 (red line) and M_∞ = 3 (black line)

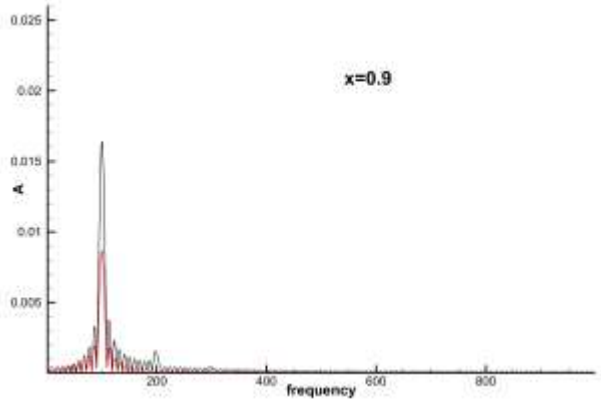

Figure 15: Amplitude spectrum of pressure *P* in a point on the vortex axis at the coordinate *x* = 0.9: incoming flow Mach number M_∞ = 2 (red line) and M_∞ = 3 (black line)

DOI: 10.13009/EUCASS2019-869

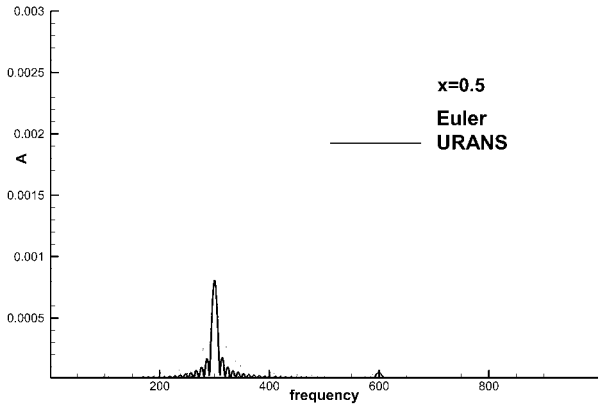

Figure 16: Amplitude spectrum of pressure P in a point on the vortex axis at the coordinate x = 0.5, incoming flow Mach number M_∞ = 3, dimensionless frequency ω = 300: URANS (solid line) and Euler (dotted line)

5. Conclusions

The results of the supersonic wingtip vortex investigation are presented in this paper. The steady state incoming flow case is investigated numerically and experimentally for Mach number M_∞ = 2, M_∞ = 3 and M_∞ = 4. The case of the presence of acoustic waves in the incoming flow is investigated numerically for Mach number M_∞ = 2 and M_∞ = 3. Acoustic perturbations were introduced in the form of monochromatic plane slow waves with small amplitude. Dimensionless frequency of introduced waves was ω = 100. Numerical simulations are carried out in the large region exceeding 30 wing chords in the framework of the URANS approach with the Spalart-Allmaras turbulence model.
The robustness of the used parallel algorithm was investigated using up to 896 cores. It is shown that the efficiency of the method does not become less than 47.8% on the grid with about 15 million cells.
Numerical and experimental data were compared for the steady state incoming flow case, and the spectral analysis of the flow results under the influence of acoustic wave disturbance was applied by using discrete Fourier transform.
The comparison of the numerical and experimental data for the steady state incoming flow shows a satisfactory agreement between the intensity, position, and size of the vortex.
The analysis of the results showed that the wingtip vortex propagates throughout the all computational domain, as well as the influence of acoustic disturbances on it. Thus, all flow parameters in the vortex don`t recover to free stream values, as well as the fluctuation amplitude of the flow parameters does not becomes zero in considered domain.
With increasing coordinate x (i.e., downstream from the wing), the intensity of the wingtip vortex decreases for all the incoming flow Mach numbers considered. This is reflected in: a decrease in the tangential Mach number in the vortex wake; a decrease in the helicity, and an increase in density and in pressure on the vortex axis. Likewise, downstream from the wing-generator (i.e. from the input boundary) the amplitude of the pressure fluctuations decreases, which is natural in view of sound absorption.
The analysis of the results showed that when the perturbation passes through the computational domain, the frequency of the first harmonic is kept equal to the frequency of the perturbation harmonic specified at the input boundary of the domain. In the middle of the region there are additional harmonics which frequencies are multiple of the first with small amplitude of little import. But by the end of the computational domain these harmonics disappear.
In the steady state incoming flow the more is the M_∞ the more intensive is the wingtip vortex, the vortex for M_∞ = 4 is most intense, for M_∞ = 2 is least intense. A similar result is observed for the case of the acoustic waves presence in the incoming flow, namely, the greater the M_∞, the greater the amplitude of the fluctuation of the gasdynamics parameters at the same distance downstream from the wing-generator at the same frequency and amplitude of the acoustic waves in the incoming flow. This is due to the higher flow rate for the greater incoming flow Mach number.
The investigation of the effect of other frequencies acoustic waves on the supersonic wingtip vortex should be the subject of further work.

6. Acknowledgments

The work was supported by the Russian Foundation for Basic Research (the projects No. 17-08-00909 and No. 19-01-00765).

DOI: 10.13009/EUCASS2019-869

References

[1] BFU. 2017. Interim Report BFU17-0024-2X. German Federal Bureau of Aircraft Accident Investigation.

[2] Giuni, M., and R.B. Green. 2013. Vortex formation on squared and rounded tip. *Aerospace Science and Technology*, 29:191-199.

[3] FAA. 1995. Wake Turbulence Training Aid (section 2). FAA Report. United States Department of Transportation.

[4] Green, S.I., and A.J. Acosta. 1991. Unsteady flow in trailing vortices. *J. of Fluid Mechanics*, 227:107-134.

[5] Spalart, Ph.R. 1998. Airplane trailing vortices. *Annual Review of Fluid Mechanics*, 30:107-138.

[6] Rossow, V. J. 1999. Lift-generated vortex wakes of subsonic transport aircraft. *Progress in Aerospace Sciences*, 35:507-660.

[7] Smart, M.K., I.M. Kalkhoran, and J. Bentson. 1995. Measurements of supersonic wing tip vortices. *AIAA J.*, 33:1761-1768.

[8] Kalkhoran, I.M., and M.K. Smart. 2000. Aspects of shock wave-induced vortex breakdown. *Progress in Aerospace Sciences*, 30:63-95.

[9] Borovoy, V.Ya., T.V. Kubyshina, A.S. Skuratov, and L.V. Yakovleva. 2000. Vortex in a supersonic flow and its influence on blunt body flow and heat transfer. *Fluid Dynamics*, 35:682-691.

[10] Shmakov, A.S., A.M. Shevchenko, A.A. Yatskikh, and Yu.G. Yermolaev. 2016. Mass flow and its pulsation measurements in supersonic wing wake. *AIP Conference Proceedings*, 1770 030019. https://doi.org/10.1063/1.4963961

[11] Shmakov, A.S., and A.M. Shevchenko. 2017. An experimental study of the vortex wake at Mach number of 3. *AIP Conference Proceedings*, 1893 030089. https://doi.org/10.1063/1.5007547.

[12] Rizzetta, D.P. 1996. Numerical investigation of supersonic wing-tip vortices. *AIAA J.*, 34:1203-1208.

[13] Kudryavtsev, A.N., S.G. Mironov, T.V. Poplavskaya, and I.S. Tsyryul'nikov. 2006. Experimental study and direct numerical simulation of the evolution of disturbances in a viscous shock layer on a flat plate. *J. of Applied Mechanics and Technical Physics*, 47:617– 627.

[14] Borovoy, V.Y., A.S. Skuratov, and E.P. Stolyarov. 2001. Pressure fluctuations in short-duration and in long-duration supersonic wind tunnels. *Uchenye zapiski TsAGI*, 32**:**3-16 (in Russian).

[15] Zinoviev, V.N., and V.A. Lebiga. 2010. Investigation of acoustic fluctuations in a flow with permeable boundaries using hot-wire anemometry. *TsAGI Science J.*, 41:133-145.

[16] Maslov, A.A., A.N. Kudryavtsev, S.G. Mironov, T.V. Poplavskaya, and I.S. Tsyryul'nikov. 2007. Numerical simulation of receptivity of a hypersonic boundary layer to acoustic disturbances. *J. of Applied Mechanics and Technical Physics*, 48:368-374.

[17] Kirilovskiy, S.V., T.V. Poplavskaya, and I.S. Tsyryulnikov. 2016. Numerical simulation of interaction of long-wave disturbances with a shock wave on a wedge for the problem of mode decomposition of supersonic flow oscillations. *AIP Conf. Proc.* (18 Int. Conf. on the Methods of Aerophysical Research (ICMAR 2016)), 1770 030040.

[18] Zhong, X. 2004. Receptivity of Mach 6 flow over a flared cone to free stream disturbance. *42nd AIAA Aerospace Science Meeting and Exhibit*. AIAA 2004-253.

[19] Borisov, V.E., A.A. Davydov, T.V. Konstantinovskaya, A.E. Lutsky, A.M. Shevchenko, and A.S. Shmakov. 2018. Numerical and experimental investigation of a supersonic vortex wake at a wide distance from the wing. *AIP Conf. Proc.* (19 Int. Conf. on the Methods of Aerophysical Research (ICMAR 2018)), 2027 030120.

[20] Landau, L.D., and E.M. Lifshitz. 1987. Course of Theoretical Physics, Fluid Mechanics. Vol 6 (2nd ed.) (Butterworth–Heinemann). ISBN 978-0-08-033933-7.

[21] www.kiam.ru

[22] Davydov, A.A., T.V. Konstantinovskaya, A.E. Lutsky, A.M. Kharitonov, A.M. Shevchenko, and A.S. Shmakov. 2013. Simulation of a supersonic flow field in the tip vortex core at the Mach number 6. *Math. Models Comput. Simul*. 5:25–36.

[23] Davydov, A.A., T.V. Konstantinovskaya, and A.E. Lutsky. 2017. Numerical simulation of a vortex wake behind a wing at a wide distance from the wing in supersonic flow. *KIAM Preprint* № 95 (2017) doi: 10.20948/prepr-2017-95.

[24] Allmaras, S.R., Johnson, F.T. and P.R. Spalart. 2012. Modifications and Clarifications for the Implementation of the Spalart-Allmaras Turbulence Model. *7th Int. Conf. on CFD* (ICCFD7), Big Island, Hawaii.

[25] Edwards, J.R., and S. Chandra. 1996. Comparison of eddy viscosity-transport turbulence models for three-dimensional, shock-separated flowfields. *AIAA J.* 34:756–763.

[26] Borisov, V.E., and A.E. Lutsky. 2016. Simulation of transition between regular and Mach shock waves reflections by an implicit scheme based on the LU-SGS and BiCGStab methods. *KIAM Preprint* № 68 (2016) doi:10.20948/prepr-2016-68 .

DOI: 10.13009/EUCASS2019-869

[27] Delery, J., E. Horowitz, O. Leuchter, and J. Solignac. 1984. Fundamental studies on vortex flows. *La Recherche Aerospatiale* (English ed.). 2:1–24.
[28] Shevchenko, A., I. Kavun, A. Pavlov, and V. Zapryagaev. 2005. Review of ITAM experiments on shock/vortex interactions. In proceedings: *European conference for aerospace sciences*, Moscow, Russia.
[29] Marks, R. J. II. 2006. The Joy of Fourier: Analysis, Sampling Theory, Systems, Multidimentions, Stochastic Processes, Random Variables, Signal Recovery, POCS, Time Scales, & Applications. Baylor University.
[30] Seregin, N. I. 2006. Special Aspects of the Use of Discrete Fourier Transform in Spectral Analysis. Ekaterinburg: Ural State Technical University manual (in Russian).
[31] Lyons, R. G. 2004. Understanding Digital Signal Processing. Prentice Hall. ISBN 0131089897.